Shot-domain 4D time-lapse seismic velocity analysis using apparent image displacements

Francesco Perrone and Paul Sava
Center for Wave Phenomena, Colorado School of Mines

ABSTRACT

Hydrocarbon production modifies the stress conditions in the subsurface and changes the model parameters previously estimated from the prospect. The capability to remotely monitor the changes in the reservoir using seismic data has strategic importance since it allows us to infer fluid movement and evolution of stress conditions, which are key factors to enhance recovery and reduce uncertainty and risk during production. A model of the subsurface parameters is necessary to reconstruct the seismic waves traveling through the medium and thus correctly image reflectors in the subsurface. Geomechanical changes in the subsurface can be measured by changes of seismic images obtained from the recorded data of multiple time-lapse surveys. In this work, we estimate changes of subsurface model parameters using the apparent shifts between migrated images obtained by 4D time-lapse seismic surveys. We assume that the shift between the time-lapse images of the same reflectors is completely due to the perturbation of the model parameters, and we use the image from the first (baseline) survey as a reference to estimate this perturbation. The apparent shifts are measured using penalized local correlations in the image domain, and they are exploited using wavefield tomography with an objective function minimized using the adjoint-state method. Our time-lapse monitoring method is efficient due to the fact that inversion can be conducted for pairs of seismic experiments, which eliminates the need to construct costly gathers. Since relatively small amounts of data are needed, our method can be used to invert for model changes at short intervals, thus increasing the resolution of 4D monitoring.

1 INTRODUCTION

Production of a hydrocarbon reservoir changes the physical parameters of the subsurface. Oil and/or gas extraction modifies the bulk modulus of the rocks and affects the geomechanics of the area. Stress changes induced by hydrocarbon production represent a key issue for constructing a geomechanical model of the reservoir. Monitoring these changes using remote sensing techniques is crucial for the oil and gas industry to design wells, predict recovery, and mitigate hazards and risk (Lumley, 2001).

Seismic waves are sensitive to the elastic properties of the subsurface. The propagation velocities of the elastic waves are directly related to to the stress state in the subsurface (Aki and Richards, 2002). By repeated seismic surveys over a reservoir at the various production stages, we can track changes in the propagation velocity in the subsurface and reconstruct the perturbation with respect to an initial model. This analysis exploits the sensitivity of the seismic waves to the elastic parameters of the subsurface. Inversion maps the changes in the recorded waveforms into a perturbation of the velocity model, which can then be related to stresses in the subsurface for geomechanical applications.

Time-lapse analysis is usually performed in the time domain (Hatchell and Bourne, 2005) and assumes small perturbations with respect to the background (baseline) model. Great care must be taken to match the baseline and monitor survey, a process called cross-equalization (Rickett and Lumley, 2001), in order to remove from the data all the differences that are not related to changes in the model parameters (e.g., differences in acquisition geometry). Similarly, time-lapse analysis can be done in the image domain, which is less sensitive to differences in the acquisition geometries and thus more robust against repeatability issues than the data domain. Shragge and Lumley (2012) propose a linearized inversion approach in the depth-domain based on the wave-equation migration velocity analysis algorithm developed by Sava and Biondi (2004). Shragge et al. (2012) apply the methodology developed by Yang and Sava (2011) to 4D seismic monitoring and uses the adjoint-state method (Fichtner et al., 2006), which removes the linearity assumptions. By operating directly in the depth domain without linearity assumptions, this inversion can handle strong errors in the velocity model.

Wave-equation MVA (Sava and Biondi, 2004) and image-domain waveform tomography (Yang and Sava, 2011) require complete aperture to correctly construct the image perturbation that drives the tomographic procedure and to evaluate fo-

cusing in the subsurface, respectively. The requirements for the acquisition geometry can be relaxed using the approach proposed by Yang and Sava (2012); nonetheless, a large aperture is necessary for resolution purposes. We advocate the use of local image correlations (Hale, 2007) to measure the relative displacement between shot-migrated images and then use the inversion technique of Perrone and Sava (2012) to evaluate a model update following production. Local image correlations allow us to estimate the velocity model errors shot by shot. The image-domain approach is robust against repeatability issues, such as errors in the shot and receiver positions, and the adjoint-state method allows us to implement a nonlinear inversion procedure, which is effective for large and complex model updates.

2 THEORY

Perrone and Sava (2012) restate the semblance principle considering locally coherent events in the image domain: the velocity model is correct when the images from different neighboring experiments show conformal features, that is, when the dips of the reflectors in the two images are point-wise consistent. This criterium can be applied to migration velocity analysis using local image correlations to evaluate the relative movement of the two images with respect to their structural dips. We can use the same idea for 4D time-lapse seismic and compare the images obtained from the baseline and monitor survey. In this case, we measure shifts of the monitor image with respect to the baseline, which represents the reference. The shift is measured along the normal to the reflector (in the dip direction).

We set an optimization problem by defining the objective function

$$\mathcal{J}(m) = \frac{1}{2} \| \sum_{\boldsymbol{\lambda}} \mathcal{P}(\mathbf{x}, \boldsymbol{\lambda})\, c(\mathbf{x}, \boldsymbol{\lambda}) \|^2_{\mathbf{x}}, \tag{1}$$

where $c(\mathbf{x}, \boldsymbol{\lambda}) = \int_{w(\mathbf{x})} R_{bsl}\left(\boldsymbol{\xi} - \frac{\boldsymbol{\lambda}}{2}\right) R_{mon}\left(\boldsymbol{\xi} + \frac{\boldsymbol{\lambda}}{2}\right) d\boldsymbol{\xi}$ is the local correlation of the baseline image $R_{bsl}(\mathbf{x})$ and the monitor image $R_{mon}(\mathbf{x})$, and $\mathcal{P}(\mathbf{x}, \boldsymbol{\lambda})$ is a penalty operator that highlights features which are related to velocity errors. The correlations are computed in local seamless overlapping windows $w(\mathbf{x})$, and the variable $m(\mathbf{x})$ denotes the model, which is slowness squared in our implementation to simplify the expression of the gradient of the objective function. When the velocity model is correct, the two images are perfectly aligned and the residual $\sum_{\boldsymbol{\lambda}} \mathcal{P}(\mathbf{x}, \boldsymbol{\lambda})\, c(\mathbf{x}, \boldsymbol{\lambda})$, a proxy for the relative displacement, is at minimum.

While we assume that the shifts between the migrated baseline and monitor survey are related to the errors in the velocity model, this is not necessarily true since changes in the stress conditions can cause compaction of the reservoir and lead to subsidence, that is physical movement of all the reflectors above the reservoir. Although subsidence up to 12 m due to hydrocarbon production has been observed and reported in the literature (for example, in the Ekofisk field in the North Sea), shifts in the subsurface are usually negligible compared to the wavelength of the seismic signal (typically these movements can be in the order of a meter between the top and bottom of the reservoir (Hatchell and Bourne, 2005)); it is thus safe to assume that the estimated shifts in the reflector positions are due to changes in the migration model and not to changes of the positions of the interfaces. This is especially true when monitor surveys are performed at short intervals, as advocated in this paper.

We compute the gradient of the objective function in equation 1 using the adjoint-state method (Fichtner et al., 2006). The migrated images are defined as the zero-lag time-correlation of the source and receiver wavefield $u_s(\mathbf{x}, t)$ and $u_r(\mathbf{x}, t)$, which are extrapolated in a model $m(\mathbf{x})$ of the subsurface. The wavefields are computed by solving the wave-equations

$$\mathcal{L}(m)\, u_s = f_s,\ \mathcal{L}(m)\, u_r = f_r, \tag{2}$$

where $\mathcal{L}(m) = m\,\partial_{tt} - \nabla^2$ is the d'Alambert operator, $f_s(\mathbf{x}_s, t)$ and $f_r(\mathbf{x}_r, t)$ are the source and the seismic reflected data, respectively, and $\mathbf{x}_s$ and $\mathbf{x}_r$ indicate the source and receiver positions. In this formulation, $m(\mathbf{x})$ represents slowness squared and since $\mathcal{L}(m)$ is linear in m, this choice simplifies the expression of the gradient of the objective function (Fichtner et al., 2006). The gradient of the objective function is

$$\nabla_m \mathcal{J} = \int (\ddot{u_s} a_s + \ddot{u_r} a_r) dt, \tag{3}$$

where the adjoint wavefields $a_s(\mathbf{x}, t)$ and $a_r(\mathbf{x}, t)$ are solutions to the wave-equations

$$\mathcal{L}^\dagger(m)\, a_s = g_s,\ \mathcal{L}^\dagger(m)\, a_r = g_r. \tag{4}$$

$\mathcal{L}^\dagger(m)$ is the adjoint of the d'Alambert operator, and the adjoint sources $g_s(\mathbf{x}, t) = \nabla_{u_s} \mathcal{J}$ and $g_r(\mathbf{x}, t) = \nabla_{u_r} \mathcal{J}$ are given by the Frechét derivatives of the objective function with respect to the background wavefields. The double dot indicates the second derivative with respect to time.

From the perspective of time-lapse analysis, the gradient $\nabla_m \mathcal{J}$ indicates which parts of the model must change in order to reduce the mismatch between the baseline and monitor migrated images. Through inversion, we can localize the areas in the model that experienced a perturbation in physical parameters and eventually relate that perturbation to geomechanical effects, such as stress changes induced by the reservoir production.

3 SENSITIVITY TESTS

We run a set of sensitivity tests to verify the behavior of the gradient computation in presence of anomalies with different signs and different sources of noise for time lapse monitoring. We verify that the gradient computation is stable when the source wavelet used for imaging is phase shifted with respect to the correct one: we use a minimum phase wavelet to image data obtained using a zero-phase wavelet. We simulate a non-repeatable survey by perturbing the positions of both sources and receivers, and we check the gradient is not

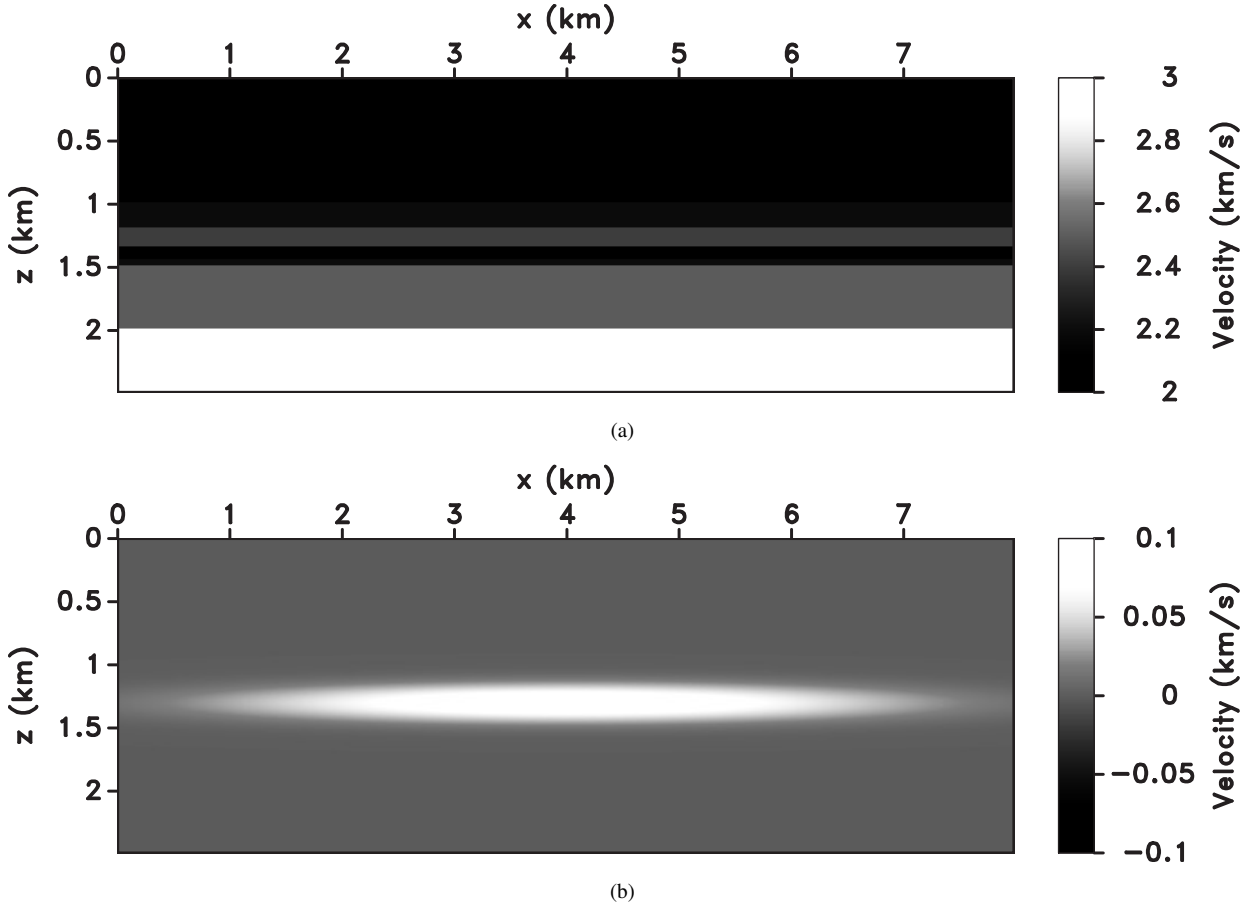

Figure 1. (a) Velocity model used to generate the data and (b) the model perturbation.

affected by source repeatability. Finally, we test the robustness of our method for errors in the baseline velocity model, and we verify that we are able to recover the relative perturbation between the baseline and monitor model.

3.1 Sensitivity to velocity variations

We generate full-acoustic finite-difference data using the velocity model in Figure 1(a). Figure 1(b) represents the velocity model perturbation due to a change in the physical parameters of the medium. The anomaly is confined to a layer and may be caused by fluid substitution or stress changes due to compaction. From an imaging perspective, these different physical phenomena translate into changes in the wave propagation velocities. The anomaly has a maximum amplitude of 0.1 km/s, which corresponds to about 5% of the background value. The vertical and horizontal sampling is 10 m and 20 m, respectively. The source function is a 15 Hz Ricker wavelet. Absorbing boundary conditions are applied so that no surface-related multiples are present in the data. We smooth the model vertically with a 10-sample triangular filter to obtain the baseline migration model.

We test the sensitivity of the algorithm to different values of the perturbation. By computing the gradient of equation 1 with the adjoint-state method from the monitor images computed using the models in Figure 2, we obtain the kernels in Figure 3. Notice that the signs of the kernels reflect the signs of the anomaly.

In a real case, the size of the anomaly would depend on the geology and geomechanics of the subsurface and also on the production activity. The link between seismic velocities and pressure in the reservoir is nonlinear, and thus it is difficult to give bounds on the minimum and maximum size of the anomaly that can be observed in the field. Also, the evolution of the anomaly as a function of time depends on the geomechanics of the area and the production activities, and these pieces of information are necessary to schedule repeated acquisition to monitor the 4D time-lapse effects.

3.2 Sensitivity to wavelet accuracy

We test the robustness of the methodology to small changes of the wavelet used for imaging. Wavelet estimation is a key step in data domain inversion techniques, but it is also quite

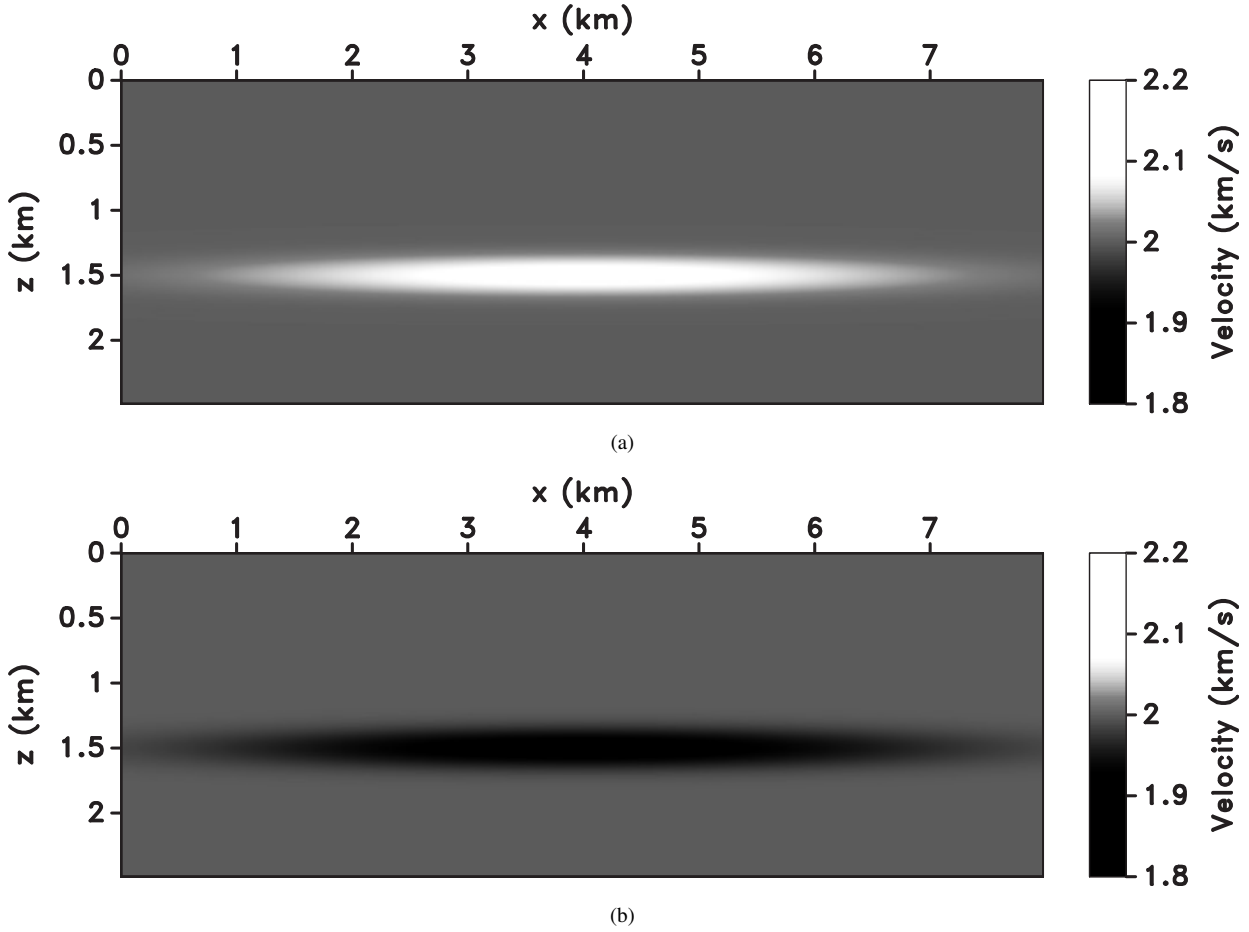

Figure 2. Velocity models with (a) positive and (b) negative anomaly with respect to a constant 2 km/s background velocity.

important when we want to estimate shifts between images of different surveys. Keeping fixed the migration velocity model, we can shift the position of the peak and trough of the wavelet superimposed on the imaged reflector by simply applying a phase-shift to the source wavelet. These shifts are unrelated to errors in the velocity model and can bias the estimate of the apparent shift between baseline and monitor image and then influence the computation of the gradient of the objective function.

Figure 4 shows (a) the wavelet used to generate the baseline and (b) the monitor data. The baseline wavelet is obtained by bandpassing the original 15 Hz Ricker wavelet using a zero-phase filter with cut-off frenquecy 15 Hz. The monitor wavelet is obtained by filtering the original Ricker wavelet in the same frequency band but using a minimum phase-filter instead. The minimum-phase filter introduces a phase shift in the wavelet that can be clearly observed in Figure 4(b).

We migrate the data with the baseline wavelet in Figure 4(a) and the two models in Figure 2. The computed gradients in Figure 5 show that for this simple case, the algorithm is robust against errors between a zero-phase and a minimum-phase source wavelet. The image shift due to errors in the source wavelet adds to the shift due to velocity errors. It is possible that the model error is small and the phase error dominates the image shift. In this latter case, the gradient would be biased. A thorough study of these possible scenarios is necessary to assess the trade-off between different sources of image displacement.

3.3 Sensitivity to survey positioning errors

Repeatability is one of the major problems in 4D time-lapse seismic processing because it is practically impossible to reproduce the same acquisition conditions over multiple surveys, and this inconsistency translates directly into differences in the acquired data that are not associated with 4D effects. We test the robustness of our inversion procedure to non-repeatability issues by randomly perturbing the positions of the source and receivers used to model the monitor data with respect to the baseline survey. The source position in the baseline survey is at $x = 3.9$ km. We record data at 100 locations evenly spaced 20 m apart starting from the source position. Figure 6 shows the baseline data, the monitor data, and their difference. Notice that the earliest events at 1.2 s and 1.3 s in the data do

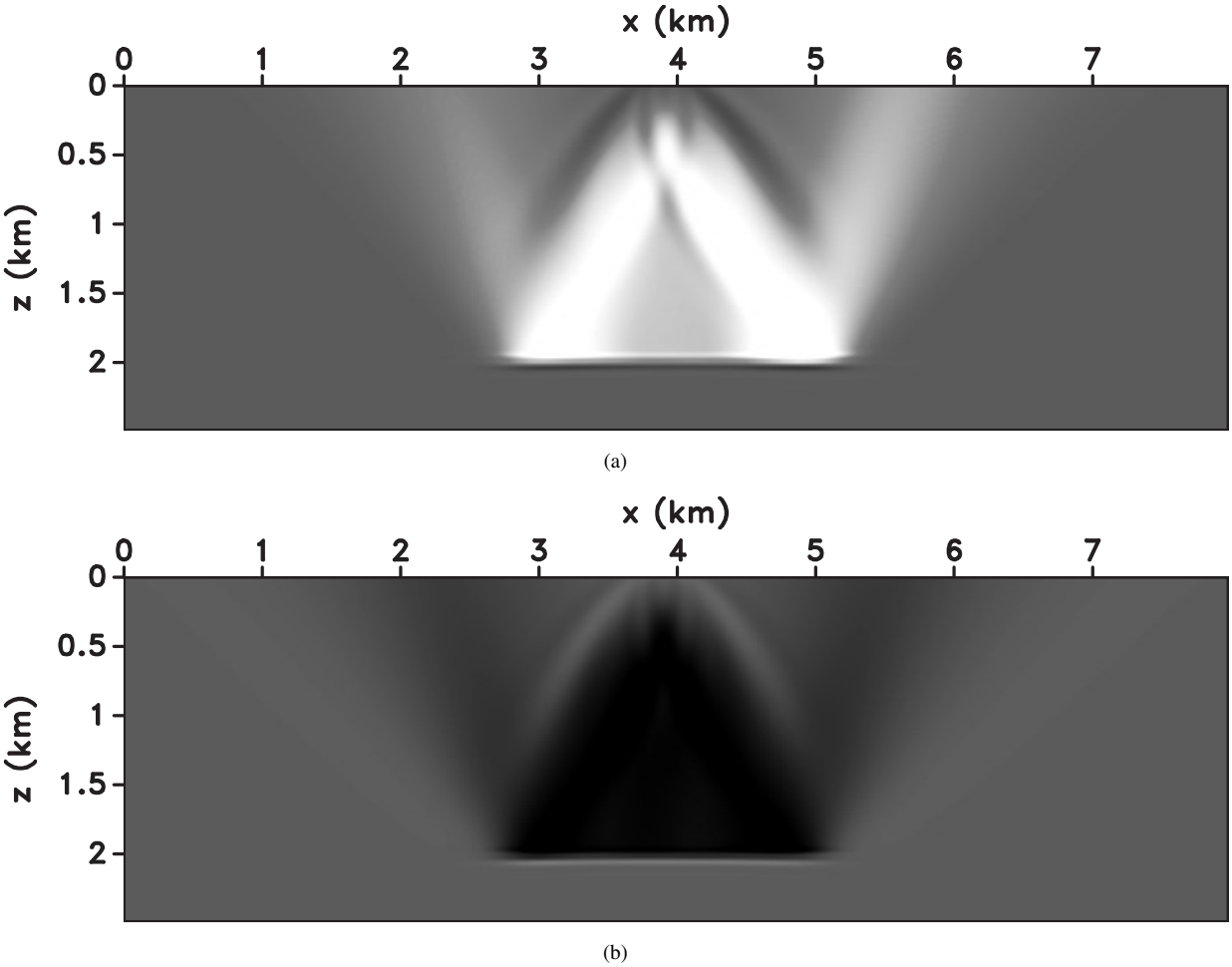

Figure 3. Gradients obtained for (a) the positive and (b) the negative anomaly in Figure 2.

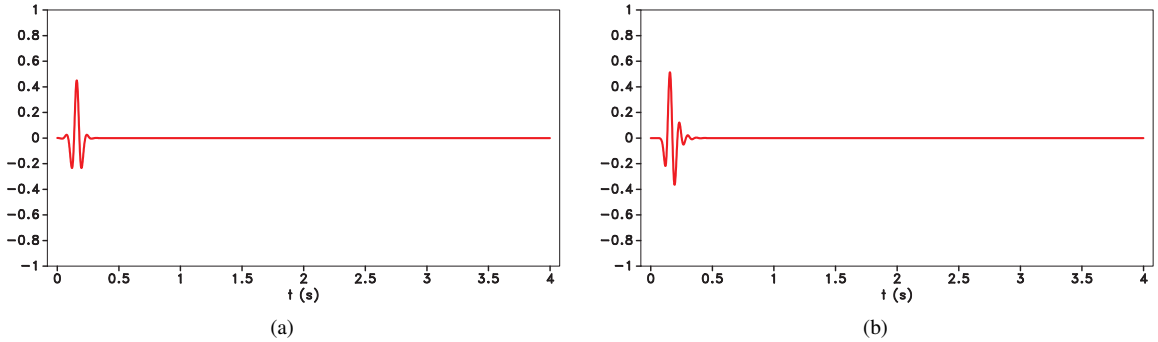

Figure 4. Wavelet for (a) the baseline and (b) the monitor survey.

not cancel because of the error in the shot position. From visual inspection, it is impossible to assess the quality of the baseline model for the monitor image; nonetheless the penalized local correlations highlight the shifts between the two images (Figure 7). Observe that the shallow reflector at 1 km depth is not affected by the anomaly, and our shift estimate correctly returns a near zero value at that location. We compute the gradient using the adjoint-state method and after 60 steepest-descent iterations, we obtain the estimated perturbation shown in Figure 8. Because of the limited aperture of the

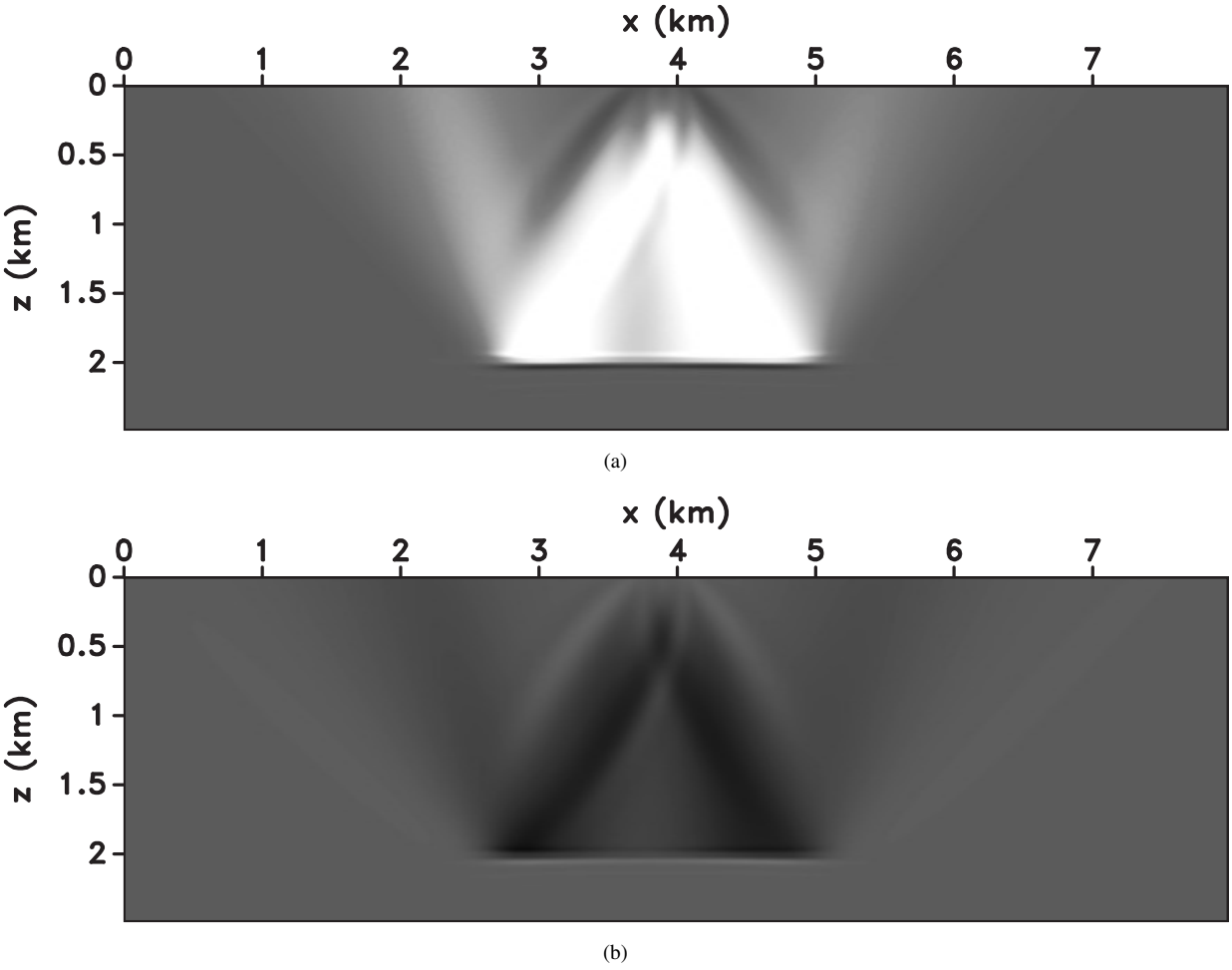

Figure 5. Gradients obtained using the minimum phase-wavelet to image zero-phase data for (a) the positive and (b) the negative anomaly in Figure 2.

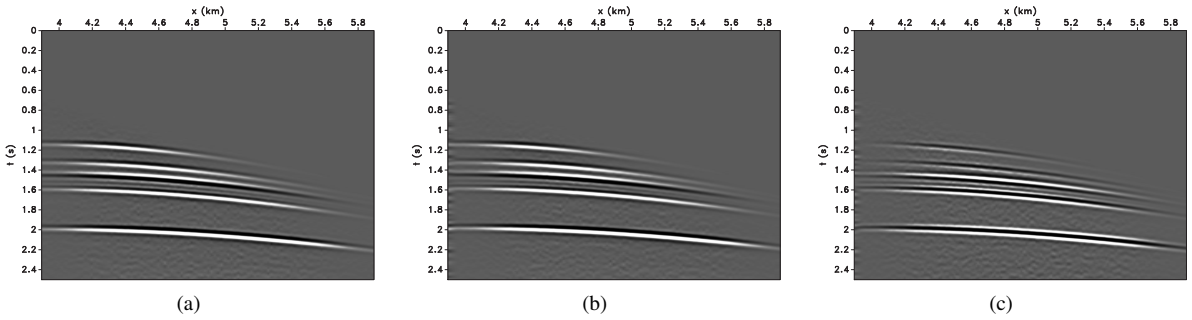

Figure 6. (a) Baseline data, (b) monitor data, and (c) data difference. Notice that because of the positioning error the events above the anomaly (at at 1.2 s and 1.3 s) do not cancel.

survey, only a portion of the anomaly is reconstructed, but the anomaly is building up in the correct layer.

3.4 Sensitivity to baseline model accuracy

Since we measure the displacement of the monitor with respect to the baseline image, we actually estimate the relative error between the monitor and baseline model. This allows us

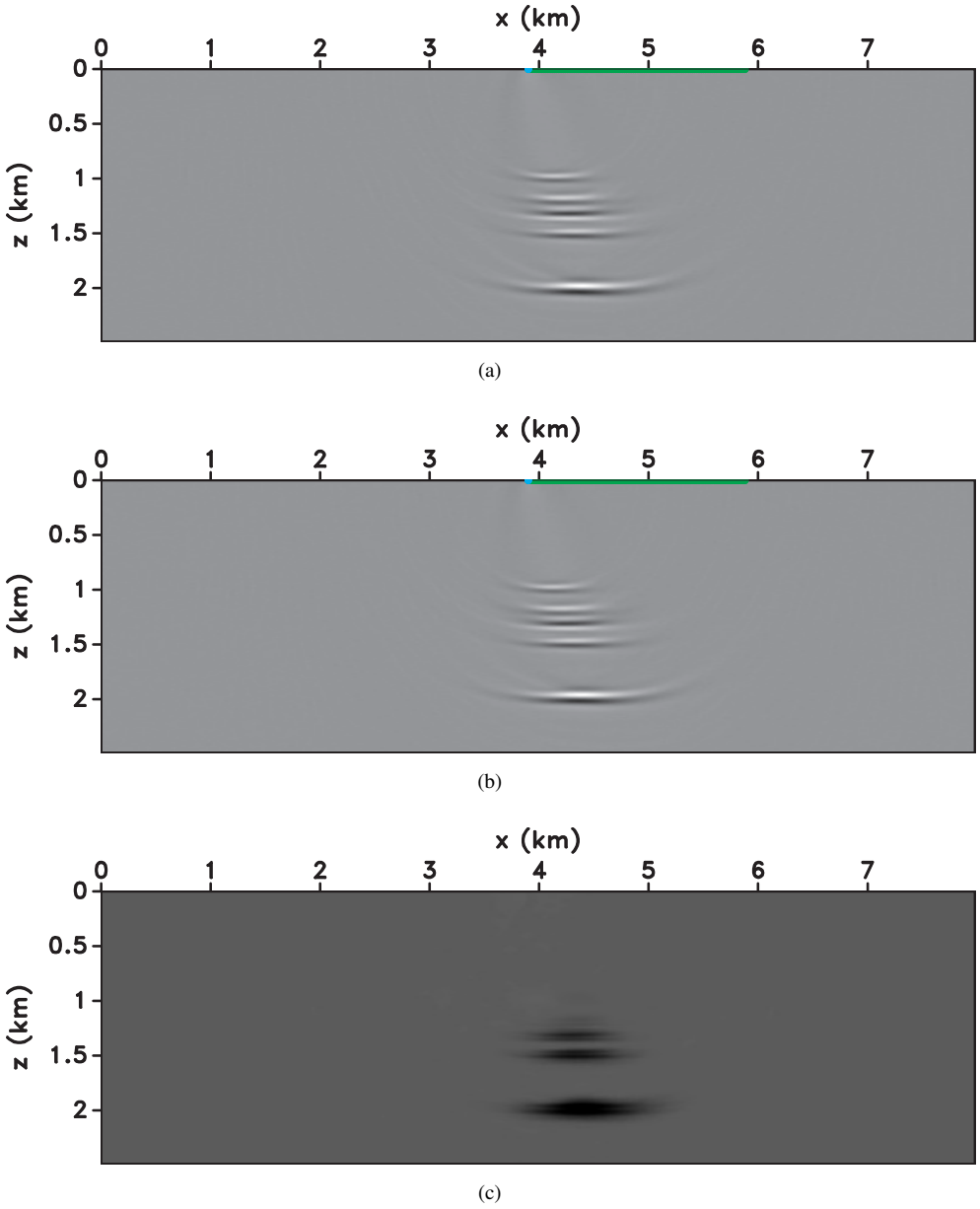

Figure 7. (a) Baseline image, (b) monitor image obtained using the baseline velocity model, and (c) relative shifts between the two images. Black indicates positive (downward) shifts and white represents negative (upward) shifts. The baseline migration model is kinematically accurate and the error is due only to 4D effects in the monitor survey.

to use a somewhat incorrect baseline model and still reconstruct the 4D changes between surveys. Figure 9 shows the baseline image, monitor image, and their relative shift if the baseline velocity model is 5% faster than the model used in Figure 7. The interfaces in both migrated images Figure 9(a) and 9(b) are mispositioned because of the bias in the baseline model. Nonetheless, the shifts only depend on the relative error between the baseline and monitor model, Figure 14(a).The result of the inversion is analogous to the case of correct baseline model, although slightly shifted in depth because of the bias in the baseline model (Figure 10).

4 SYNTHETIC RESERVOIR DEPLETION MODEL

When a reservoir is produced, the depletion causes geomechanical effects both inside and outside the reservoir. Because of the drop in pore pressure, the reservoir rock compacts and the effective stress (and seismic velocity) increases; outside

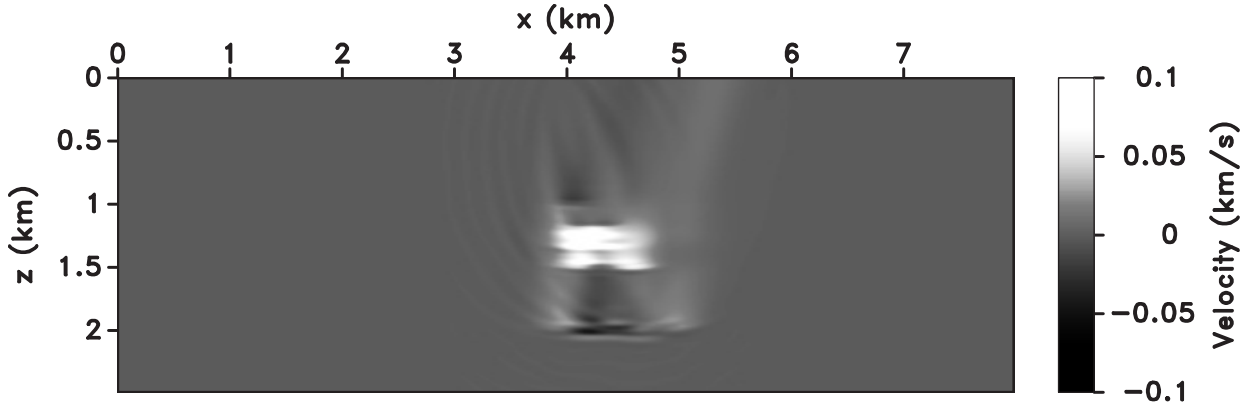

Figure 8. Estimated perturbation after 60 tomographic iterations with a correct baseline velocity model.

the reservoir the rock is strained and the seismic velocity decreases. This observed phenomenon can be analyzed using time-shifts (Hatchell and Bourne, 2005; Hale et al., 2008; Smith and Tsvankin, 2012) and describes the complex changes in subsurface stress conditions caused by oil and gas production.

In order to test our velocity estimation procedure in a more realistic scenario, we use a geomechanical model designed by Smith and Tsvankin (2012) to obtain the model parameters for a reservoir under depletion. We generate data with acoustic finite-differences using density reflectors at various depths and with absorbing boundary conditions on each side of the model (Figure 11(a)). The initial velocity model is homogenous and equal to 2.07 km/s velocity. Figure 11(b) shows the model of the reservoir undergoing a 15% depletion. Observe the complex pattern of the velocity anomaly outside the reservoir. The velocity model perturbation inside the reservoir is about $+15\%$ with respect to the baseline model. Figure 12 shows the data obtained for the baseline and monitor surveys. Observe the internal multiples arriving after 2.5 s and following the strong deeper reflection. From visual inspection, it is difficult to notice any shift in the waveform. However, because of the opposite sign of the velocity anomaly, the early arrivals (around 1.2 s) are delayed and the late waveforms (after 1.5 s) are advanced in time.

Our inversion experiment uses a single shot gather with the source located at $x = 1.5$ km and with a streamer 3.2 km long. The length of the cable is about the same as the lateral extent of the reservoir. The streamer carries 300 evenly spaced receivers and the receiver spacing is 8 m. The gradient of the objective function is smoothed using a triangular filter with radius 2 samples vertically and 5 samples horizontally. The model is updated using a steepest descent algorithm. We implement regularization through triangular smoothing. The smoothing procedure acts as regularization in the inversion by removing spurious high wavenumber sidelobes in the gradient. More sophisticated and structure oriented regularization approaches can be used for more complex subsurface scenarios.

Figure 13 shows the true perturbation and the result of our single-shot inversion after 60 tomographic iterations. Because of the limited aperture of the acquired data, the wavefields are not sensitive to the complete extent of the anomaly. Nonetheless, the imaged portion of the model allows us to constrain the size and location of the anomaly. Notice that the inversion is able to recover the weaker perturbation outside the reservoir of opposite sign with respect to the perturbation within the reservoir, and observe that we are also able to correctly image the left side of the anomaly thus correctly constraining its lateral extent.

Figure 14 shows the shifts between the baseline and monitor migrated images before and after inversion. Black indicated a downward shift whereas white indicate an upward whift. Before inversion the shallower and deeper reflectors are shifted in opposite direction because of the different sign of the anomaly inside and outside the reservoir (see Figure 13(a)). After inversion the reflectors are better aligned and the shifts for all reflectors approach zero. Inversion warps the monitor image into the baseline image and returns the velocity anomaly that corrects the shifts of the imaged interfaces.

5 DISCUSSION

The change of physical properties (such as wave propagation velocity) due to reservoir production leads to apparent shifts in the migrated images obtained from repeated time-lapse seismic surveys of the field. Because the velocity model used in migration is calibrated on the baseline survey, the monitor survey reflectors are slightly mispositioned since we are not taking into account the perturbation of the model due to the production of the field. By matching the baseline and monitor migrated images for single shots, we can translate the apparent image shift into a model perturbation. This approach is fully shot-based since the basic building blocks of the inversion procedure are the single-shot migrated images. This feature is advantageous in a real production scenario when it is difficult to repeat a complete survey because of physical obstructions in the field (such as platforms) which can cause big illumination

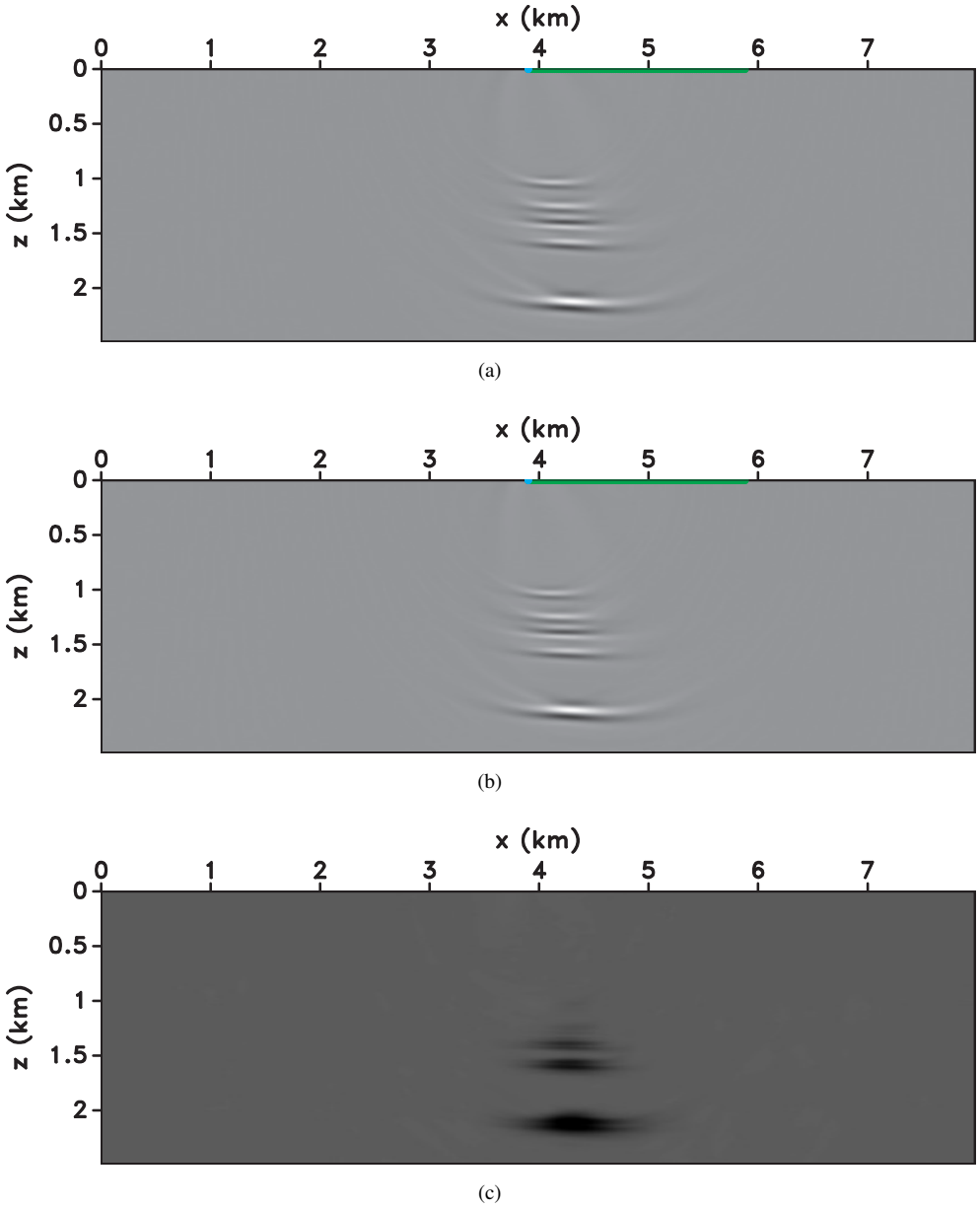

Figure 9. (a) Baseline image, (b) monitor image obtained using the baseline velocity model, (c) relative shifts between the two images. Black indicates positive (downward) shifts and white represents negative (upward) shifts. Here, the migration velocity model is 5% faster than the correct one.

holes in the images. Conducting a complete survey over a producing field is also costly because production must be stopped during acquisition in order to reduce the noise in the seismic data. Our technique addresses this practical problem and can potentially allow for fast and frequent surveys over a producing reservoir.

The advantage of our technique over methods based on wavefield focusing (Girard and Vasconcelos, 2010; Shragge et al., 2012) comes from the reduced implementation cost (no extended images are needed) and the robustness against poor illumination. By analyzing single-shot migrated images, we are automatically taking into account the illumination pattern of those experiments; on the contrary, focusing measures require full aperture or point-spread function compensation to equalize the complex illumination patterns due to the geologic structures and/or acquisition geometry. In this work, we recover a portion of the anomaly from a *single* migrated shot, which would be impossible using any technique based on focusing.

In general, velocity anomalies due to reservoir stimula-

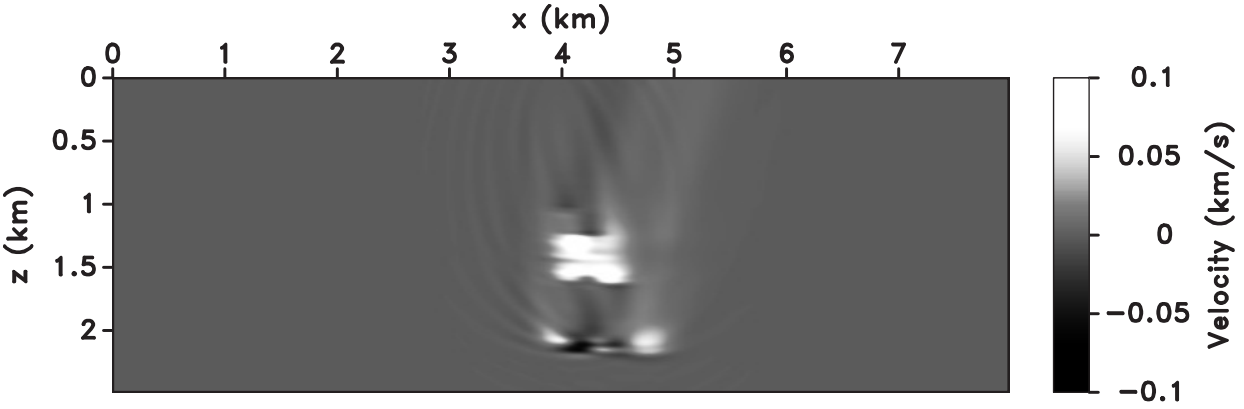

Figure 10. Estimated perturbation after 60 tomographic iterations with an incorrect baseline velocity model.

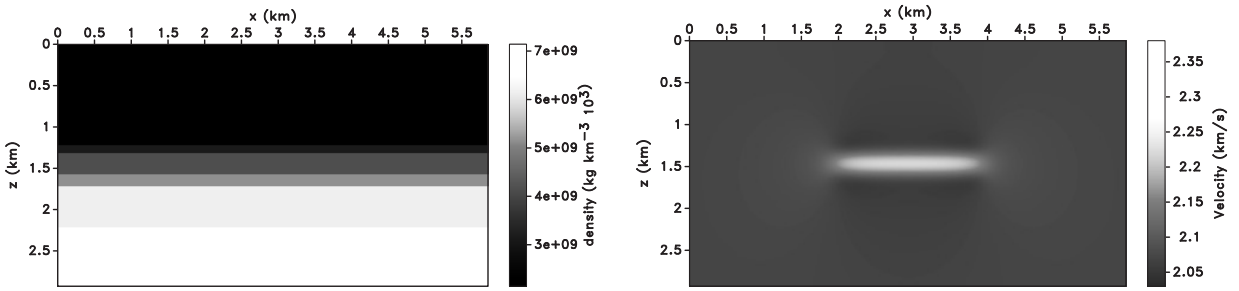

(a) (b)

Figure 11. (a) Density model used to simulate the reflecting interfaces. (b) Velocity model of the depleted reservoir. The original model is homogenous with 2.07 km/s velocity. Observe the characteristic shape of the anomaly with increasing velocity inside the reservoir (because of compaction) and decreasing velocity outside the reservoir (because of strain).

tion or production are small relative to the velocity error in the initial stages of model building. Moreover, the baseline velocity model should already be calibrated and thus be expected to produce a high-quality migrated image. Therefore, our technique based on apparent image shifts is more robust for time-lapse seismic monitoring than for the original migration velocity analysis, when we match a set of inaccurate images.

6 CONCLUSIONS

Local correlations evaluated in the image domain allow us to assess the quality of the velocity model from a limited number of migrated images. In 4D seismic applications, we can quickly estimate a perturbation of the migration model by comparing shot images from baseline and monitor surveys. In the image domain, we measure the consistency and similarity of locally coherent events, like the local dip of the reflectors; these features are weakly sensitive to differences in the acquisition geometry and make our approach more robust against survey repeatability issues as compared to alternative strategies in the data domain. The method is able to recover the relative error in the model and does not require separate velocity analysis for baseline and monitor surveys in order to estimate the differences between the models inverted independently.

7 ACKNOWLEDGMENTS

We would like to thank Jyoti Behura for interesting discussions about 4D time-lapse seismic and for encouraging FP to look into this problem. This work was supported by the sponsors of the Consortium Project on Seismic Inverse Methods for Complex Structures. The reproducible numerical examples in this paper use the Madagascar open-source software package freely available from http://www.ahay.org and the Mines JTK freely available at https://github.com/dhale/jtk.

REFERENCES

Aki, K., and P. G. Richards, 2002, Quantitative seismology: University Science Books.

Fichtner, A., H.-P. Bunge, and H.Igel, 2006, The adjoint method in seismology I. theory: Physics of the Earth and Planetary Interiors, 86–104.

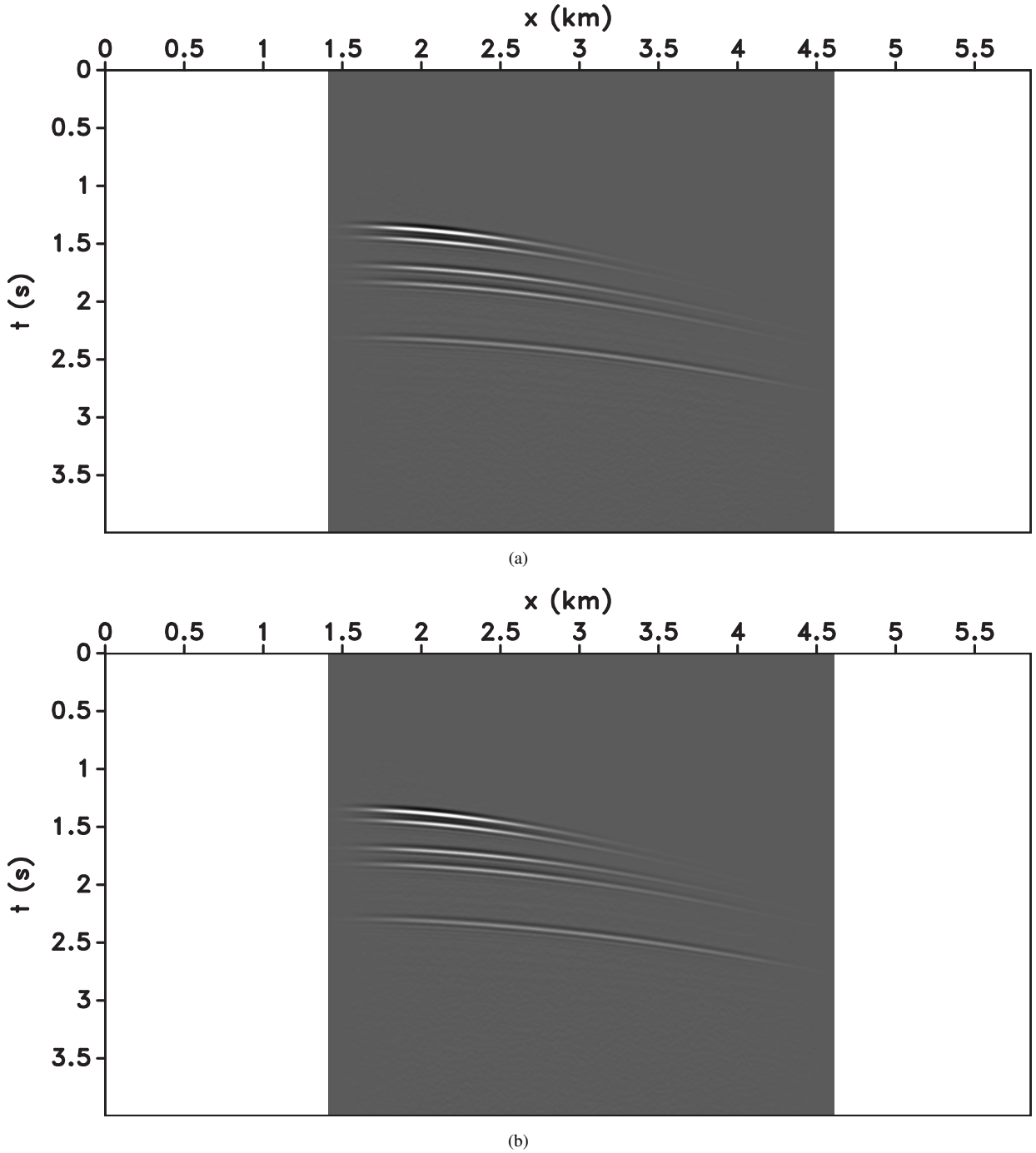

Figure 12. (a) Baseline data and (b) monitor data simulated in the depleted reservoir. By inspection, it is impossible to observe any perturbation in the arrival times.

Girard, A., and I. Vasconcelos, 2010, Image-domain time-lapse inversion with extended images: Presented at the 80th Ann. Internat. Mtg., Soc. of Expl. Geophys.

Hale, D., 2007, A method for estimating apparent displacement vectors from time-lapse seismic data: Technical Report CWP-566, Center for Wave Phenomena, Colorado School of Mines.

Hale, D., B. Cox, and P. J. Hatchell, 2008, Apparent horizontal displacements in time-lapse seismic images: Presented at the SEG Technical Program Expanded Abstracts, SEG.

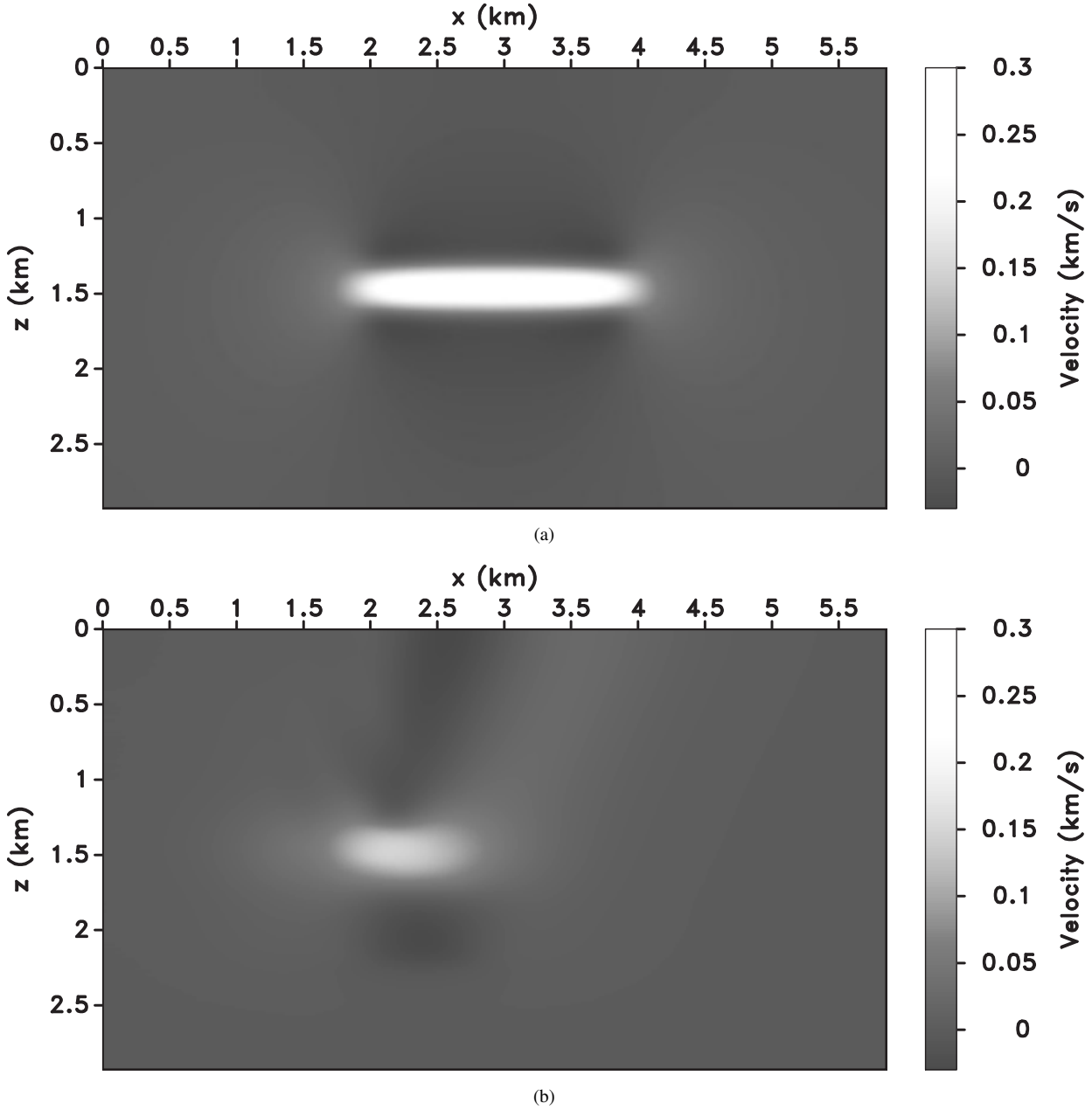

Figure 13. (a) Real time-lapse model perturbation and (b) inverted perturbation after 60 iterations of wavefield tomography. Notice that we are able to correctly image the anomaly and also constrain its lateral extent at about $x = 2$ km.

Hatchell, P. J., and S. J. Bourne, 2005, Measuring reservoir compaction using time-lapse timeshifts: Presented at the 75th Ann. Internat. Mtg., Soc. of Expl. Geophys.

Lumley, D. E., 2001, Time-lapse seismic reservoir monitoring: Geophysics, **66**, 50–53.

Perrone, F., and P. Sava, 2012, Wavefield tomography based on local image correlation: Presented at the 74th Conference and Exhibition, EAGE.

Rickett, J. E., and D. E. Lumley, 2001, Cross-equalization data processing for time-lapse seismic reservoir monitoring: A case study from the Gulf of Mexico: Geophysics, **66**.

Sava, P., and B. Biondi, 2004, Wave-equation migration velocity analysis. I. Theory: Geophysical Prospecting, **52**, 593–606.

Shragge, J. C., and D. E. Lumley, 2012, 4D seismic wave-equation depth migration velocity analysis: Presented at the 74th Conference and Exhibition, EAGE.

Shragge, J. C., T. Yang, and P. Sava, 2012, Time-lapse image-

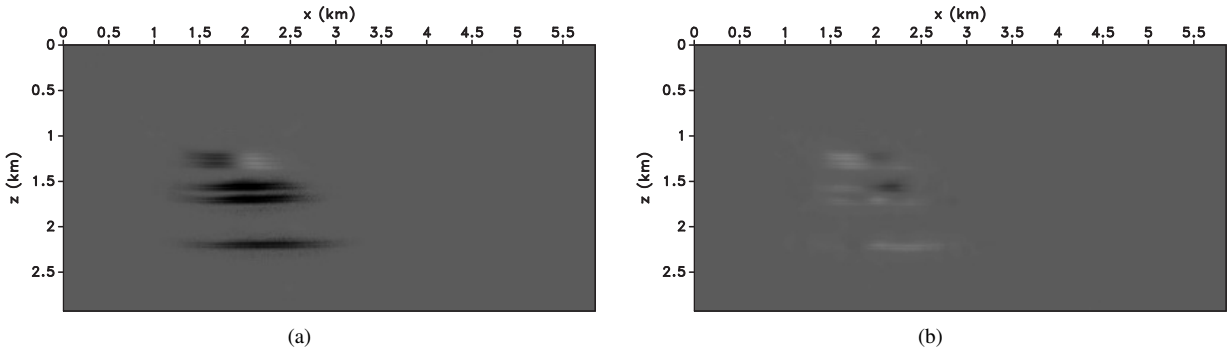

Figure 14. (a) Initial estimated shifts and (b) estimated shifts after 60 iterations of wavefield tomography. Black indicates positive (downward) shifts and white represents negative (upward) shifts. Inversion matches the baseline and monitor images and reduces the shifts between them.

domain velocity analysis using adjoint-state methods: Presented at the SEG Technical Program Expanded Abstracts, Soc. of Expl. Geophys.

Smith, S. S., and I. Tsvankin, 2012, Modeling and analysis of compaction-induced traveltime shifts for multicomponent seismic data: Geophysics, **77**, T221–T237.

Yang, T., and P. Sava, 2011, Image-domain waveform tomography with two-way wave-equation: Presented at the 81th Ann. Internat. Mtg., Soc. of Expl. Geophys.

———, 2012, Illumination compensation for image-domain wavefield tomography: Presented at the 74th Conference and Exhibition, EAGE.